Journal Pre-proof

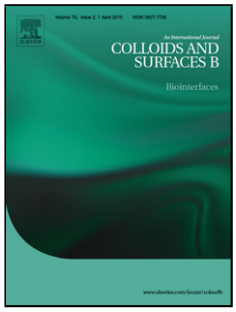

Macrophage inflammatory and metabolic responses to graphene-based nanomaterials differing in size and functionalization

Mónica Cicuéndez, Márcia Fernandes, Miguel Ayán-Varela, Helena Oliveira, María José Feito, Rosalía Diez-Orejas, Juan I. Paredes, Silvia Villar-Rodil, Mercedes Vila, M. Teresa Portolés, Iola F. Duarte

PII: S0927-7765(19)30853-7

DOI: https://doi.org/10.1016/j.colsurfb.2019.110709

Reference: COLSUB 110709

To appear in: *Colloids and Surfaces B: Biointerfaces*

Received Date: 12 August 2019

Revised Date: 13 November 2019

Accepted Date: 4 December 2019

Please cite this article as: Cicuéndez M, Fernandes M, Ayán-Varela M, Oliveira H, Feito MJ, Diez-Orejas R, Paredes JI, Villar-Rodil S, Vila M, Portolés MT, Duarte IF, Macrophage inflammatory and metabolic responses to graphene-based nanomaterials differing in size and functionalization, *Colloids and Surfaces B: Biointerfaces* (2019), doi: https://doi.org/10.1016/j.colsurfb.2019.110709

Macrophage inflammatory and metabolic responses to graphene-based nanomaterials differing in size and functionalization

Mónica Cicuéndez[1,2,*], Márcia Fernandes[1], Miguel Ayán-Varela[3], Helena Oliveira[1,4], María José Feito[5], Rosalía Diez-Orejas[6], Juan I. Paredes[3], Silvia Villar-Rodil[3], Mercedes Vila[2], M.Teresa Portolés[5], Iola F. Duarte[1,*]

[1]CICECO-Aveiro Institute of Materials, Department of Chemistry, University of Aveiro, 3810-193 Aveiro, Portugal.
[2]NRG-TEMA, Department of Mechanical Engineering, University of Aveiro, 3810-193 Aveiro, Portugal.
[3]Instituto Nacional del Carbón, INCAR-CSIC, C/Francisco Pintado Fe 26, 33011 Oviedo, Spain.
[4]Department of Biology & CESAM, University of Aveiro, 3810-193 Aveiro, Portugal.
[5]Department of Biochemistry and Molecular Biology, Faculty of Chemistry, Universidad Complutense de Madrid, Instituto de Investigación Sanitaria del Hospital Clínico San Carlos (IdISSC), Ciudad Universitaria s/n, 28040 Madrid, Spain.
[6]Department of Microbiology and Parasitology, Faculty of Pharmacy, Universidad Complutense de Madrid, 28040 Madrid, Spain.

[*]Corresponding authors: ioladuarte@ua.pt; mcicuendez@ucm.es

Graphical abstract

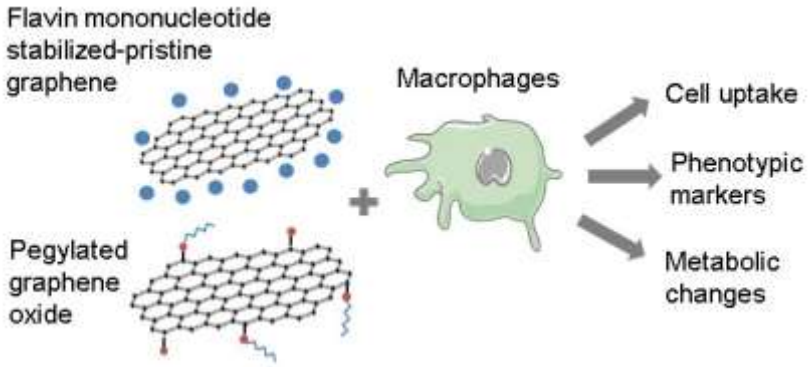

Highlights

- Uptake of graphene nanomaterials (GBN) by macrophages was mainly determined by size.
- Macrophage inflammatory activation depended also on nanomaterial functionalization.
- Flavin mononucleotide-pristine graphene induced pro-inflammatory metabolic changes.
- Pegylated graphene oxide nanosheets showed low inflammatory potential.
- Tuning of GBN size and functionalization can be used to modulate macrophage activation.

Abstract

The preparation of graphene-based nanomaterials (GBNs) with appropriate stability and biocompatibility is crucial for their use in biomedical applications. In this work, three GBNs differing in size and/or functionalization have been synthetized and characterized, and their *in vitro* biological effects were compared. Pegylated graphene oxide (GO-PEG, 200–500 nm) and flavin mononucleotide-stabilized pristine graphene with two different sizes (PG-FMN, 200–400 nm and 100–200 nm) were administered to macrophages, chosen as cellular model due to their key role in the processing of foreign materials and the regulation of inflammatory responses. The results showed that cellular uptake of GBNs was mainly influenced by their lateral size, while the inflammatory potential depended also on the type of functionalization. PG-FMN nanomaterials (both sizes) triggered significantly higher nitric oxide (NO) release, together with some intracellular metabolic changes, similar to those induced by the prototypical inflammatory stimulus LPS. NMR metabolomics revealed that macrophages incubated with smaller PG-FMN displayed increased levels of succinate, itaconate, phosphocholine and phosphocreatine, together with decreased creatine content. The latter two variations were also detected in cells incubated with larger PG-FMN nanosheets. On the other hand, GO-PEG induced a decrease in the inflammatory metabolite succinate and a few other changes distinct from those seen in LPS-stimulated macrophages. Assessment of TNF-α secretion and macrophage surface markers (CD80 and CD206) further corroborated the low inflammatory potential of GO-PEG. Overall, these findings revealed distinct phenotypic and metabolic responses of macrophages to different GBNs, which inform on their immunomodulatory activity and may contribute to guide their therapeutic applications.

Keywords

Graphene oxide, pristine graphene, flavin mononucleotide, macrophages, inflammatory response, metabolomics

1. Introduction

In recent years, graphene-based nanomaterials (GBNs) have attracted considerable attention as promising tools in the field of biomedicine, and have been proposed for several applications, such as contrast imaging, drug and gene delivery, or anticancer hyperthermia.[1,2] Most of these biomedical applications demand intravenous injection of GBNs, which raises concerns about their safety and potential health risks. The toxic effects of GBNs are influenced by multiple factors, such as concentration, purity, lateral dimension, surface structure, oxidation level, functionalization and the dispersion method used in their preparation.[3-6] Thus, careful scrutiny of the impact of well-characterized GBNs on human cells is essential to understand their mechanisms of action and to contribute to their risk-benefit assessment.[7]

Graphene oxide (GO) is currently the most widely explored GBN for health-related applications.[8] GO can be described as graphene where oxygen-containing functional groups have been introduced, namely carboxylic and carbonyl groups on the edges, and hydroxyl and epoxy groups on the basal plane. The high density and diversity of oxygen functional groups on the GO surface provide reactive sites for chemical functionalization with biocompatible polymers, such as polyethylene glycol (PEG). This modification increases GO colloidal stability in physiological conditions, minimizes interactions with other biomolecules, and reduces the risk of adverse immunological responses.[9]

Over the past few years, direct exfoliation of graphite in the liquid phase has been proposed as a simple and efficient alternative to obtain graphene for different applications.[10] Pristine graphene (PG) is a two-dimensional analogue of graphite, which, unlike GO, totally lacks functional groups. The hydrophobicity of PG hinders its colloidal dispersion in water and aqueous biological media, making its functionalization necessary

for incorporation into biological systems. Several surfactants or stabilizers have been used in graphite exfoliation and colloidal stabilization in aqueous medium, including ionic[11] and non-ionic/polymeric surfactants[12], dye or fluorescence molecules[13] and large biomolecules[14]. Recently, our research group has shown that flavin mononucleotide (FMN), an innocuous derivative of riboflavin (vitamin B_2), is a high-performing biodispersant for graphene flakes.[10] The assessment of biological responses to these novel FMN-stabilized PG nanomaterials (PG-FMN) is now crucial for their further progress towards specific biomedical applications.

Macrophages are highly plastic innate immune cells which play a key role in the processing of nanomaterials, from their blood clearance and *in vivo* trafficking[15,16] to the initiation and coordination of inflammatory immune responses.[17] Furthermore, the modulation of macrophage polarization by nanomaterials is currently viewed as a promising adjuvant approach to influence site-specific inflammation, particularly with regard to the tumour microenvironment.[18] Hence, the response of macrophages to nanomaterials is an important facet of their biological performance. Cell metabolism has recently emerged as a key axis of macrophage activation, with pro- and anti-inflammatory phenotypes (often designated as M1- and M2-like) being characterized by distinct metabolic programs.[19,20] NMR metabolomics is a particularly powerful tool to investigate macrophage metabolic modulation by nanomaterials, as it enables the direct detection of metabolites identified as inflammatory response markers (e.g. succinate and itaconate), as well as of unanticipated changes in central metabolic pathways, potentially providing novel insights into cell-nanomaterial interactions at the molecular level.[21-23]

In the present work, we have evaluated the cellular uptake, inflammatory potential and metabolomic profile of macrophages exposed to thoroughly characterized GBNs differing in their size and/or functionalization: GO-PEG and PG-FMN (L), both with

lateral sizes in the 200 - 500 nm range, and PG-FMN (S), with lateral sizes from 100 to 200 nm. This research aims at correlating important biological endpoints with key physicochemical properties of GBNs and is expected to advance current understanding of the immunomodulatory activity of these materials.

2. Materials and methods

2.1. Synthesis and characterization of GBNs

For the synthesis of PG, graphite powder was added to an aqueous FMN solution (1 mg/mL) at a mass ratio of 30:1 and the ensuing mixture was sonicated in an ultrasound bath for 5 h (J. P. Selecta Ultrasons system; frequency: 40 kHz; power: ~20 W L^{-1}). The resulting suspension was divided into two portions of equal volume and each was subjected to centrifugation for 20 min to sediment poorly exfoliated or non-exfoliated particles. Two different centrifugal forces were used, 500 and 3,000*g*, to obtain PG-FMN (L) and PG-FMN (S), respectively. The top ~75% of the supernatant volume was collected as graphene dispersion for further use. To remove the free, non-absorbed FMN molecules from the resulting dispersions, they were purified through iterative cycles of sedimentation via centrifugation (20,000*g*, 20 min), replacement of two thirds of the resulting supernatant solution by milli-Q water and re-dispersion of the sedimented flakes in this new solution by a brief (2 min) sonication step.

The samples were characterized by UV-vis absorption (extinction) spectroscopy, X-ray photoelectron spectroscopy (XPS), Raman spectroscopy and scanning transmission electron microscopy (STEM). UV-vis absorption/extinction spectra were recorded on a double-beam Heλios α spectrophotometer (ThermoSpectronic) with an optical path length of 1 cm. XPS measurements were carried out on a SPECS system under a pressure of 10^{-7} Pa with a non-monochromatic Mg K_α X-ray source operated at 11.81 kV and 100

W. Raman spectroscopy was accomplished with a Horiba Jobin-YvonLabRam apparatus at a laser excitation wavelength of 532 nm. Specimens for both Raman and XPS analysis were prepared by drop-casting aqueous graphene dispersions onto a metallic sample-holder pre-heated at ~50–60 ºC and allowing them to dry under ambient conditions until a uniform film covered the substrate. STEM images were acquired on a Quanta FEG 650 system (FEI Company) operated at 30 kV. Specimens for STEM were prepared by mixing equal volumes of the aqueous graphene dispersion and ethanol. Then, 40 μL of the resulting suspension was drop-cast onto a copper grid (200 square mesh) covered with a continuous carbon film (Electron Microscopy Sciences) and allowed to dry under ambient conditions.

Graphene oxide (GO) was obtained through exfoliation of graphite oxide resulting from oxidation of high-purity graphite in an acidic medium, by a modified Hummers method, as previously reported.[24] The suspension of GO nanosheets was dialyzed until pH 7 and activated with chloroacetic acid under strongly basic conditions (NaOH) to promote −COOH groups at the surface. GO was then functionalized by covalent bonding [diimide activation by adding 1-Ethyl-3-(3-dimethylaminopropyl) carbodiimide hydrochloride (EDAC)] with the non-toxic and non-immunogenic polymer Poly(Ethylene Glycolamine) (PEG), to improve coloidal stability and minimize immunogenicity. Pegylated GO nanosheets were marked with the amine reactive dye fluorescein isothiocyanate (FITC), covalently bound to PEG. The resulting samples were analyzed by Atomic Force Microscopy (AFM) in a *multimode* Nanoscope III A Bruker system. Dynamic light scattering (DLS) measurements of colloidal dispersions (pH 5) were performed in a ZetasizerNano series instrument equipped with a 633 nm "red" laser (Malvern Instruments). Z-average sizes of three sequential measurements were collected at room temperature (RT). X-Ray Photoelectron Spectroscopy (XPS) spectra were

acquired in a Ultra High Vacuum (UHV) system with a base pressure of 2×10^{-10} mbar. The GO-PEG powder was dispersed in milli-Q water and drop-cast onto a Si wafer. The system was equipped with a hemispherical electron energy analyzer (SPECS Phoibos 150), a delay-line detector and a monochromatic Al K_α (1486.74 eV) X-ray source.

2.2. Cellular uptake of GBNs

RAW-264.7 macrophages were seeded at 10^5 cells/mL in Dulbecco's Modified Eagle Medium (DMEM) supplemented with 10% fetal bovine serum (FBS, Gibco), 1 mM L-glutamine (BioWhittaker Europe), penicillin (200 µg/mL) and streptomycin (200 µg/mL, BioWhittaker Europe), and cultured for 24 h at 37 ºC under a 5% CO_2 atmosphere. Then, 10 µg/mL of either GO-PEG-FITC, PG-FMN (L) or PG-FMN(S) dispersed in culture medium were added to the cell culture, and cells were incubated for additional 24 h under the same conditions. The concentration of GBNs was selected based on a preliminary assessment of cell viability, using the trypan blue dye exclusion assay. The results showed that cell viability was above 70% upon macrophage incubation with 10 µg/mL of either GO-PEG or PG-FMN nanosheets, which, according to the norm ISO 10993-5:2009(E),[25] can be considered non-cytotoxic. Controls without nanomaterials were always carried out in parallel. To evaluate the incorporation of GBNs by RAW-264.7 macrophages, cells were washed with phosphate-buffered saline (PBS), harvested using cell scrapers and analyzed by flow cytometry. The fluorescence of GO-PEG-FITC was excited at 488 nm and measured with a 530/30 band pass filter in a Coulter XL Flow Cytometer (Beckman Coulter). For PG-FMN (L) and PG-FMN (S) nanomaterials, cellular uptake was evaluated using flow cytometric light scatter analysis in a Coulter XL Flow Cytometer (Beckman Coulter) equipped with an argon ion laser (15 mW, 488 nm). The light scattered at an angle of 90°, designated as the side angle scatter (SSC), is proportional to

the intracellular complexity, while the laser light collected at small scatter angles, called forward angle scatter (FSC), is proportional to the cell size. Thus, this is a simple method to evaluate the uptake of nanomaterials by mammalian cells.[26] All acquisitions were made using SYSTEM II software v. 3.0 (Beckman Coulter). For each sample, 10,000–60,000 cells were analysed at a flow rate of about 1,000 cells/s.

2.3. Nitric oxide production

The amount of nitrite in the culture medium was measured as an indicator of nitric oxide (NO) production by macrophages using the Griess assay. RAW-264.7 macrophages were seeded at a density of 10^5 cells/mL in complete DMEM, under a 5% CO_2 atmosphere and at 37ºC for 24 h. Then, GBNs (10 µg/mL) or LPS (1 µg/mL) were added to the cell culture and, after a 24 h incubation, 100 µL of culture medium was collected from each well and mixed with 100 µL of Griess reagent (Sigma-Aldrich, catalogue no. G4410). The mixture was incubated for 15 min at RT and protected from light, after which the absorbance at 540 nm was measured in a microplate reader. Unstimulated controls incubated under the same conditions were also measured.

2.4. NMR metabolic profiling

To assess macrophage metabolic composition, cells were seeded in 100 mm diameter dishes at a density of 1.5×10^6 cells per dish and cultured in complete DMEM. After 24h, the medium was replaced by fresh medium containing each GBN at 10 µg/mL (or 1 µg/mL LPS) and incubated for additional 24 h. For each condition (control, LPS, GO-PEG, PG-FMN (S) and PG-FMN (L)), three replicate dishes were cultured. To collect cell samples, the medium was aspirated, and each dish was quickly washed four times with PBS, to completely remove all medium, while preserving intracellular composition.

Then, intracellular aqueous metabolites were extracted using a dual-phase extraction, with methanol/chloroform/water (1:1:0.7), as previously described.[27] At the time of NMR analysis, dried polar extracts were reconstituted in 600 μL of deuterated phosphate buffer (100 mM, pH 7.4) containing 0.1 mM TSP-d_4, and 550 μL of each sample were transferred to 5 mm NMR tubes.

NMR spectra were acquired on a Bruker Avance III HD 500 spectrometer operating at 500.13 MHz for ^{1}H observation, at 298 K, using a 5 mm TXI probe. Standard 1D spectra with water suppression (pulse program 'noesypr1d', Bruker library) were acquired with 32 k data points, a spectral width of 7002.8 Hz, a 2 s relaxation delay and 2048 scans. Spectral processing comprised FID exponential multiplication with a 0.3 Hz line broadening factor, zero filling to 64 k data points, manual phase, baseline correction and calibration to the TSP-d_4 signal at 0 ppm. Spectral assignment was based on 2D total correlation spectroscopy (TOCSY), *J*-resolved and heteronuclear single quantum coherence (HSQC) spectra and consultation of spectral databases, such as the Bruker Biorefcode database and the human metabolome HMDB database.[28]

To assess the magnitude of metabolite variations, selected spectral peaks were integrated in Amix-viewer (Bruker, version 3.9), and normalized by the total area of each spectrum (excluding the suppressed water signal). This normalization procedure was carried out to compensate for differences in cell density, thus allowing for signal intensities to be compared between samples. For each metabolite, the magnitude of variation relatively to controls was assessed by calculating the effect size (ES), adjusted for small sample numbers, and respective standard error.[29] The metabolic changes with absolute ES larger than 0.8 (and with standard error < ES) were graphically represented by a heatmap, which was color-coded according to the percentage of variation in relation to untreated control cells.

2.5. Immunocytochemistry of GO-PEG-exposed macrophages

RAW-264.7 macrophages were seeded in 6-well culture plates at 10^5 cells/mL, in complete DMEM and cultured for 24 h at 37 ºC under a 5% CO_2 atmosphere. Then, GO-PEG-FITC dispersed in culture medium was added to the cell culture and cells were incubated for either 24 h or 48 h at 37 ºC under a 5% CO_2 atmosphere. Controls without GO-PEG-FITC were cultured in parallel. Expression of cell surface markers CD80 and CD206, typically increased in pro-inflammatory and anti-inflammatory macrophages respectively,[30,31] was then assessed. After detachment and centrifugation, and before adding the primary antibody, cells were incubated in 45 µL of staining buffer (PBS, 2.5% FBS from Gibco and 0.1% sodium azide from Sigma-Aldrich) with 5 µL of normal mouse serum inactivated for 15 min at 4ºC, in order to block the Fc receptors on the macrophage plasma membrane, and to prevent non-specific binding. Then, cells were incubated with either phycoerythrin (PE) conjugated anti-mouse CD80 antibody (2.5 µg/mL, BioLegend) or PE conjugated anti-mouse CD206 (2.5 µg/mL, BioLegend) for 30 min in the dark. Labelled cells were analyzed using a FACS Calibur flow cytometer. PE fluorescence was excited at 488 nm and measured at 585/42 nm. The conditions for data acquisition and analysis were established using negative and positive controls with the CellQuest Program of Becton Dickinson, and these conditions were maintained in all the experiments. Each experiment was carried out three times and single representative experiments are displayed. For statistical significance, at least 10,000 cells were analyzed in each sample and the mean of the fluorescence emitted by those single cells was used. Furthermore, the amount of TNF-α in the culture medium was quantified by ELISA (Gen-Probe, Diaclone), according to the manufacturer`s instructions.

2.6. Statistics

Univariate statistical analysis was performed using the Statistical Package for the Social Sciences (SPSS) version 19 software. Data were expressed as mean ± standard deviation, with n ≥3. Statistical significance was assessed through the student t-test or one-way ANOVA (for multiple comparisons). Scheffé test was used for *post hoc* evaluation of differences among groups. For all comparisons, FDR-adjusted p-values were calculated using the R software version 3.4.1. (R Core Team (2017). R: A language and environment for statistical computing. R Foundation for Statistical Computing, Vienna, Austria. http://www.R-project.org/). Differences were considered statistically significant for $p < 0.05$.

3. Results and discussion

3.1. GBNs characterization

The pristine graphene (PG) dispersions studied in the present work were obtained by FMN-assisted exfoliation and colloidal stabilization of graphite powder in aqueous medium. Bath sonication of graphite powder in FMN aqueous solution followed by centrifugation and purification yielded opaque, black-colored dispersions indicative of successful exfoliation, which displayed long-term colloidal stability. Two different centrifugation speeds were employed, namely 500 and 3,000*g*, to obtain the nanomaterials henceforth designated as PG-FMN (L) and PG-FMN (S), respectively. The former value (500*g*) falls within the optimal range previously determined for this parameter,[10,32] which afforded sedimentation of poorly or non-exfoliated graphite particles, while maximizing the concentration of material that is colloidally stable in the long-term (few months). The latter centrifugal force (3,000*g*) is expected to lead to additional sedimentation of thicker and/or larger exfoliated graphene flakes, thus

producing a dispersion with a different population of flakes in terms of size/thickness compared to that obtained at 500*g*.

The UV-vis spectra of the purified dispersions (**Figure 1A**) displayed strong absorbance in the visible and near-infrared range, consistent with the opacity and black tone of the dispersions, as well as an UV absorption maximum at ~ 270 nm, attributed to $\pi \rightarrow \pi^*$ transitions in extended electronically conjugated carbon structures. All these features are typical of pristine graphene dispersions[12,33] and confirm the successful exfoliation in water of bulk graphite. The additional sedimentation that takes place at a centrifugal force of 3,000*g* explains the lower absorbance (thus, lower concentration) displayed by the resulting dispersion (green trace in **Figure 1A**). The average thickness of dispersed graphene flakes could also be inferred from UV-vis data, according to the empirical formulae proposed by Backes *et al.*.[34] Based on the intensity ratio of extinction at 550 nm to extinction at 325 nm, the two PG-FMN dispersions were found to have ~10 monolayers, and thus, comparable thickness. The lateral dimensions of the flakes were directly measured from STEM images (**Figure1 B-E**). Both dispersions were seen to comprise lamellar objects (**Figure 1B** and **1C**), and, as expected, the dispersion centrifuged at 500*g* contained flakes of larger sizes. Histograms showing lateral size distributions of PG-FMN (L) and PG-FMN (S) are displayed in **Figure 1D** and **1E**, respectively. Typical values ranged between 100 nm and 1 μm for PG-FMN (L) (~55% of the objects between 200 and 400 nm) and 100–400 nm for PG-FMN (S) (~55% objects between 100 and 200 nm).

Raman spectroscopy was employed to gain structural insight into the FMN-dispersed graphene flakes. **Figure 1F** shows representative Raman spectra of films prepared from aqueous dispersions of PG-FMN (L) (red traces) and PG-FMN (S) (green traces) flakes. The spectrum of the starting graphite is also shown for comparison (black

trace). In the first-order region (1100–1800 cm^{-1}), the spectra were dominated by the G band characteristic of graphitic materials, located at ~1580 cm^{-1}, while the defect-related D (~1348 cm^{-1}) and D' (~1620 cm^{-1}) bands[35,36] were rather weak. This indicates that the exfoliated materials possessed a relatively high structural quality. The average integrated intensity ratio of the D and G bands (I_D/I_G ratio), which is usually taken as a quantitative measure of the structural disorder present in graphite/graphene materials, was ~0.2 and ~0.3 for PG-FMN (L) and PG-FMN (S), respectively. We note that for the calculation of the I_G value (integrated intensity of the G band), we excluded the contribution of the D' band, which appears as a shoulder on the high wavenumber side of the G band. The slight increment in I_D/I_G values of the exfoliated materials, relative to that of the starting graphite material (I_D/I_G~0.1), can be attributed to the smaller size of the flakes, which brings about an increased fraction of edges, rather than due to defects within the basal plane. Indeed, the height ratio of the D and D' bands ($H_D/H_{D'}$ ratio), which has been correlated with the type of predominant defect in graphene,[37] displayed an $H_D/H_{D'}$ ratio of ~5, consistent with the preponderance of graphitic edges for both materials.[38] Furthermore, the same value of $H_D/H_{D'}$ was found for the starting graphite, which implies that the exfoliation process did not introduce new types of defect in the graphene flakes. The second-order Raman spectra were dominated by the 2D (or G') band, located at ~2700 cm^{-1}. However, the shape and position of this band, known to depend on the stacking order and number of layers of graphene materials, changed remarkably with exfoliation. The 2D band of the starting graphite material was markedly asymmetrical, while that of the exfoliated materials was symmetrical and down-shifted, consistent with the presence of few-layer graphene flakes.

Chemical information on the dispersed flakes was gathered by XPS. **Figure 1G** displays normalized C 1s core level spectra of films prepared from aqueous graphene

dispersions PG-FMN (L) (red trace) and PG-FMN (S) (green trace). For comparison, the spectrum recorded for the starting graphite is also presented (black trace). The spectrum corresponding to PG-FMN (L) (red trace) was nearly coincident with that of the starting graphite, implying that the chemical nature of the bulk parent material remained virtually intact upon exfoliation. However, the spectrum of the film prepared from the PG-FMN (S) dispersion showed a slightly lower intensity at binding energy (BE) of ~284.6 eV, which corresponds to non-oxidized, graphitic environment, and higher intensity at higher BEs, corresponding to oxidized carbon atoms. Rather than arising from oxidation of the carbon framework upon exfoliation, we believe that this small difference stems from the presence of some marginal amount of FMN adsorbed on the graphene surface.

The pegylated GO nanomaterial was characterized by AFM, XPS, zeta-potential (ζ) and DLS particle size analysis. The chemical exfoliation of graphite in aqueous media, followed by chemical activation and size separation by centrifugation, resulted in nanosheets with an average thickness of ~9 nm, corresponding to 13–14 layers, as assessed by AFM (**Figure 2A**). Moreover, based on DLS data, the nanosheets displayed sizes in the 200–500 nm range (**Figure 2B**). Although DLS is not ideal for size determination of non-spherical particles, it has been widely applied in the characterization of graphene nanosheets and shown to correlate well with TEM results.[39,40] Also, it should be noted that the size estimate provided by DLS was corroborated by AFM data. Pegylated GO was also characterized by XPS to study the elemental composition and chemical environment of the elements present at its surface. **Figure 2C** shows a fitted C 1s spectrum, composed of four components centered at: 284.8 eV (C-C/C=C), 286.3 eV (C-O/C-N), 287.7 eV (C=O) and 288.9 eV (O-C=O/N-C=O). In general, the treatment carried out to promote the carboxylation of GO hydroxyl and epoxide groups diminished the intensity of the peak of the C 1s spectrum associated to C–O groups (at 286.3 eV).

Thus, the high intensity of this peak after the pegylation process indicates successful incorporation of PEG-diamine. On the other hand, the N 1s spectrum (**Figure 2D**) showed a maximum at 400.0 eV, assigned to C–N in amine and amide groups of PEG-diamine bound to GO. Given the asymmetry of the spectrum, an additional component at 401.7 eV, attributed to protonated amine groups from PEG-diamine,[41] was included in the deconvolution scheme. The results confirm the success of the pegylation procedure. Finally, zeta-potential analysis was carried out to evaluate GO's surface charge. According to previously published data, the zeta-potential of chemically activated GO with -COOH surface groups was -38±8 mV.[24] In the present study, after the pegylation process, the zeta-potential value changed slightly to -32±6 mV, which is consistent with the presence of amino ended branches.

3.2. Cellular uptake of GBNs

Macrophages play a key role during the host immune response in many different physiological contexts. Concerning nanomaterials, these cells are primarily responsible for their uptake and trafficking *in vivo*.[42] In the present study, the uptake of GBNs by RAW-264.7 macrophages was studied by flow cytometry after 24 h of incubation.

Figure 3A shows the side angle scatter profiles (SSC-A) and the mean SSC (inset) of RAW-264.7 macrophages cultured in the presence of PG-FMN (L) or PG-FMN (S) compared to control cells. The SSC profiles after treatment with PG-FMN (L) (orange) or PG-FMN (S) (green) showed clear displacements towards higher values relatively to control cells (blue). These corresponded, respectively, to ~30% and ~83% significant increments of the intracellular complexity of exposed macrophages, compared to controls. Also, cells cultured with PG-FMN (S) showed SSC values significantly higher than macrophages cultured with PG-FMN (L), indicating greater cellular incorporation

of PG-FMN (S) compared to PG-FMN (L). This agrees with previous reports where cell uptake of GBNs was shown to critically depend on their size, among other properties.[43,44] The incorporation of GO-PEG-FITC nanomaterial by RAW-264.7 macrophages was evaluated using fluorescence intensity profiles, after adding trypan blue to quench the fluorescence produced by the GO-PEG-FITC adsorbed on the outer surface of cells (**Figure 3B**). In this case, a significant increment in the fluorescence intensity issued by GO-PEG-exposed macrophages (blue profile) was observed when compared to control cells (red profile), indicating the presence of this nanomaterial inside cells.

A complementary flow cytometric light scatter analysis was carried out in order to compare the cellular uptake of the two nanomaterials with similar lateral size distributions, PG-FMN (L) (200–400 nm) and GO-PEG (200–500 nm). The results showed similar SSC profiles and no significant differences in the mean SSC of macrophages exposed either to PG-FMN (L) or GO-PEG nanomaterials **(Supplementary Figure S1)**. Moreover, a significant SSC increase of RAW cells cultured with PG-FMN (S) was observed in comparison to macrophages cultured with PG-FMN (L) or GO-PEG. Altogether, these results indicate that the cellular uptake of the different GBNs evaluated, *i.e.*, PG-FMN (L), PG-FMN (S) and GO-PEG, was mostly determined by the lateral size and not by the chemical modification of these nanomaterials.

3.3. Effect of GBNs on nitric oxide production

In response to pro-inflammatory stimuli like LPS, macrophages typically increase the production of nitric oxide (NO) through enzymatic metabolization of arginine by nitric oxide synthase.[45] In this study, macrophage incubation with LPS induced a 30% increase in NO production relative to unstimulated control cells (**Figure 4**). As for GBNs, GO-PEG did not induce NO production, whereas PG-FMN (S) and PG-FMN (L) caused

significant NO increases of 21% and 12%, respectively. These results clearly suggest that GO-PEG has a lower inflammatory potential then PG-FMN nanomaterials.

3.4. Effect of GBNs on macrophage metabolome

In order to obtain further insight into the cellular effects of the different GBNs tested, the metabolic composition of GBNs-exposed macrophages, as well as of LPS-treated macrophages (M1) and untreated control cells, was assessed by ^{1}H NMR spectroscopy. A representative cells spectrum is shown in **Figure 5A** and detailed spectral assignment is provided in **Supplementary Table S1**.

Based on spectral integration, metabolite variations induced by GO-PEG, PG-FMN (S) and PG-FMN (L) were quantitatively assessed in relation to untreated control cells, as summarized in the form of a heatmap (**Figure 5B**). Metabolite variations induced by the prototypical pro-inflammatory stimulus LPS were also assessed for comparison. As expected, LPS-treated macrophages displayed significantly increased levels of succinate and itaconate, together with decreased fumarate, reflecting TCA cycle rewiring to support the inflammatory response.[46,47] Intracellular succinate accumulation in LPS-treated macrophages has been attributed to inhibition of succinate dehydrogenase (SDH),[48] and directly linked to stabilization of the transcription factor HIF-1α, together with increased production of reactive oxygen species (ROS) and the pro-inflammatory cytokine IL-1β.[49] On the other hand, citrate-derived itaconate is currently recognized as an anti-inflammatory metabolite, which counter balances inflammation mainly by activating the transcription factor Nrf2 and restricting excessive production of pro-inflammatory molecules.[50] Interestingly, among the GBNs tested, only PG-FMN (S) caused increases in intracellular succinate and itaconate, similarly to LPS, while PG-FMN (L) did not alter the levels of TCA cycle intermediates. On the other hand, macrophages

exposed to GO-PEG displayed decreased succinate and increased fumarate compared to control cells, suggesting increased flux through SDH. Treatment with LPS also affected the levels of several amino acids. Branched chain amino acids and glutamine increased, which could reflect increased consumption from the culture medium and/or protein catabolism, whereas glutamate and aspartate decreased, likely reflecting their use as TCA cycle anaplerotic substrates.[20] As for GBNs, they barely affected amino acid levels, the only alteration being noted for leucine and isoleucine in GO-PEG-exposed macrophages (**Figure 5B**).

The cellular levels of glutathione (GSH) were decreased in both LPS- and GBN-treated macrophages compared to untreated control cells (**Figure 5B**). This tripeptide (Glu-Cys-Gly) acts as a cofactor for some antioxidant enzymes and neutralizes reactive oxygen species (ROS), thus being a key antioxidant molecule in cells. Oxidative stress is one of the primarily proposed mechanisms of graphene toxicity, which can damage proteins, DNA and lipids, leading to progression of several harmful effects.[51] The observed GSH decrease in GBN-treated macrophages corroborates the activation of this endogenous antioxidant system to cope with GBN-induced ROS. In the case of LPS-treated cells, additional decreases were found for taurine and β-alanine, which may also act as antioxidant metabolites. Rattigan *et al.* also observed that β-alanine metabolism was significantly altered in LPS-activated macrophages.[52]

Other metabolic effects shared by LPS and PG-FMN (both sizes) comprised an increase in phosphocreatine and a decrease in creatine. These metabolites are interconvertible through a reaction catalysed by the enzyme creatine kinase (CK) and play an important role in temporal and spatial energy buffering, as ATP can be rapidly recycled from the breakdown of phosphocreatine into creatine and inorganic phosphate.[53] Differentiated macrophages were shown to develop a large phosphocreatine pool, used

up during phagocytosis.[54] On the other hand, Leishmania-infected macophages[55] and macrophages incubated with either silk fibroin nanoparticles[23] or ultra small superparamagnetic particles of iron oxide[21] displayed increased phosphocreatine levels. The results of the present study suggest that PG-FMN, but not GO-PEG, also interfered with the creatine kinase/phospohocreatine system in RAW 264.7 macrophages. One may speculate that macrophage exposure to PG-FMN could have possibly impaired CK-mediated phosphocreatine to creatine conversion (leading to accumulation of the former and depletion of the latter), a hypothesis which warrants further investigation. Interestingly, the inhibitory effect of nanomaterials towards this enzyme has been previously reported for brain and skeletal muscle CK exposed to silver nanoparticles.[56]

Finally, we also noticed prominent variations in choline-containing metabolites (**Figure 5B**). Phosphocholine increased upon exposure to LPS or to PG-FMN (S), and an additional strong increase in glycerophosphocholine was noticed in LPS-treated macrophages. As these compounds are important constituents of membrane phospholipids, such increases could reflect membrane degradation. On the other hand, GO-PEG-treated macrophages displayed decreased phosphocholine levels, as compared to untreated controls, which could reflect lower membrane turnover. In line with these findings, graphene nanoplatelets with lateral size in the range of several hundred nanometers to several micrometers were also reported to alter the metabolism of glycerolipids, glycerophospholipids, and sphingolipids in macrophages.[57]

Altogether, the metabolic responses of macrophages to the different GBNs tested in our study suggest a lower pro-inflammatory potential of GO-PEG, as compared to PG-FMN, corroborating the results of the Griess assay (see section 3.3).

3.5. Phenotypic characterization of GO-PEG-exposed macrophages

In order to further confirm the low pro-inflammatory potential of GO-PEG, TNF-α secretion and M1/M2 cell surface markers were evaluated in macrophages exposed to GO-PEG for 24 and 48 h. The production of the pro-inflammatory cytokine TNF-α was significantly lower in cells treated with GO-PEG for 24 h than in control macrophages, although no differences were observed for 48 h treatments (**Figure 6A**).

Regarding the prototypical M1-like surface marker CD80, there was no difference in the percentage of the $CD80^+$ population in control and 24 h GO-PEG-exposed cells (28 ± 4.3% *vs*. 27 ± 4.8%) (**Figure 6B, left**). The results also showed that, within exposed $CD80^+$ cells, 36% of the population incorporated GO-PEG. After 48 h, the percentage of cells expressing CD80 ($CD80^+$ population) decreased in both control and GO-PEG-exposed groups (**Figure 6B, right**). Moreover, within GO-PEG-exposed cells, 90% of the $CD80^+$ population incorporated GO-PEG, indicating an increase of GO-PEG uptake over culture time, as seen by others for different cells types and nanomaterials.[24] The surface marker CD206, typically upregulated in M2-like macrophages,[31] showed low expression in both control and GO-PEG-exposed macrophages (0.8 ± 0.2% and 1.6 ± 0.3%, respectively), with no significant difference between them after 24 h (**Figure 6C, left**). However, after 48 h, CD206 expression increased in both control and GO-PEG-exposed macrophages, but more prominently in the latter, leading to a statistically significant difference (1.5 ± 0.3% *vs*. 2.2 ± 0.5%) (**Figure 6C, right**). It is also interesting to note that 100% of $CD206^+$ GO-PEG-exposed macrophages incorporated GO-PEG. Overall, these results further corroborate that GO-PEG did not induce pro-inflammatory macrophage activation, which is in good agreement with the results obtained in a previous work for primary macrophages exposed to the same GO-PEG formulation.[58]

4. Conclusions

In summary, we have shown that the lateral dimensions and functionalization of GBNs differently affected their biological performance, as assessed *in vitro* using a macrophage cell line. Cellular uptake was determined mostly by size, with smaller particles showing greater internalization, while inflammatory activation additionally depended on the surface-modifying agent employed. Based on phenotypic features and intracellular metabolic changes, PG-FMN nanomaterials, especially of smaller size, were found to induce macrophage pro-inflammatory responses (e.g. enhanced nitric oxide production, increased intracellular succinate, itaconate, phosphocholine and phosphocreatine), while GO-PEG did not trigger this kind of activation. These findings indicate that tuning of GBN size and functionalization can potentially be used to modulate macrophage activation. Overall, given the increasingly recognized role of these cells in host responses to foreign materials, as well as in the pathogenesis and progression of several diseases, this work reinforces the promising potential of GBNs in biomedical applications.

Author's contribution statement

All authors have contributed significantly to the work. Author contributions were as follows: S.V.-R., M.A.-V. and J.I.P. synthetized and characterized PG-FMN nanomaterials; M.V. and M.C. synthetized and characterized GO-PEG; H.O. performed cell uptake measurements by flow cytometry; T.P., M.J.F. and R.D.-O. performed phenotypic characterization of GBN-exposed macrophages; M.F., M.C. and I.F.D. recorded and analysed NMR metabolic profiles; M.C. and I.F.D. conceived the study and wrote the manuscript, with contributions from the other co-authors.

Competing interests statement

There are no competing interests to declare.

Acknowledgements

This work was developed in the scope of the projects CICECO-Aveiro Institute of Materials, FCT Ref. UID/CTM/50011/2019, and CESAM, FCT Ref. UID/AMB/50017/2019, financed by national funds through FCT/MCTES. The research grant from the Spanish Ministerio de Economía y Competitividad (MAT2016-75611-R AEI/FEDER, UE) is also acknowledged. Further ackwoledgments are due to the Portuguese NMR (PTNMR) Network, supported with FCT funds, Bruker BioSpinGmbH and the European Union Framework Programme for Research and Innovation HORIZON 2020, under the TEAMING Grant agreement No 739572 - The Discoveries CTR. I.F.D. and H.O. acknowledge FCT/MCTES for research contracts under the Programs 'Investigador FCT' and Stimulus to Scientific Employment (CEECIND/04050/2017), respectively. M.C. acknowledges the financial support from FCT (SFRH/BPD/101468/2014). M.A.-V., S.V.-R. and J.I.P. acknowledge financial support from the Spanish Ministerio de Economía y Competitividad (MINECO) and the European Regional Development Fund (ERDF) through project MAT2015-69844-R, and from the Spanish Ministerio de Ciencia, Innovación y Universidades, the Spanish Agencia Estatal de Investigación and ERDF, through project RTI2018-100832-B-I00. Partial funding by Plan de Ciencia, Tecnología e Innovación (PCTI) 2013-2017 del Principado de Asturias and the ERDF (project IDI/2018/000233) is also acknowledged. Thanks also to the staff of the Centro de Citometría y Microscopía de Fluorescencia of the Universidad Complutense de Madrid (Spain) and ICTS Centro Nacional de Microscopia Electrónica (Spain) for assistance in the flow cytometry and AFM studies, respectively.

References

1. C. McCallion, J. Burthem, K. Rees-Unwin, A. Golovanov, A. Pluen, *Eur. J. Pharm. Biopharm.*, 2016, **104**, 235–250.

2. M. Cicuéndez, J. Flores, H. Oliveira, M.T. Portolés, M. Vallet-Regí, M. Vila, I.F. Duarte, *Mater. Sci. Eng. C*, 2018, **91**, 340-348.

3. A.B. Seabra, A.J. Paula, R. de Lima, O.L. Alves, N. Durán, *Chem. Res. Toxicol.*, 2014, **27**, 159–168.

4. F.M. Tonelli, V.A. Goulart, K.N. Gomes, M.S. Ladeira, A.K. Santos, E. Lorençon, L.O. Ladeira, R.R. Resende, *Nanomedicine*, 2015, **10**, 2423–2450.

5. D. Bitounis, H. Ali-Boucetta, B.H. Hong, D.H. Min, K. Kostarelos, *Adv. Mater.*, 2013, **25**, 2258–2268.

6. A. Bianco, *Angew. Chem. Int. Ed.*, 2013, **52**, 4986–4997.

7. X. Hu, Q. Zhou. *Chem. Rev.*, 2013, **113**, 3815–3835.

8. S. Syama, P.V. Mohanan, *Int. J. Biol. Macromol.*, 2016, **86**, 546–555.

9. G. Gonçalves, M. Vila, M.T. Portolés, M. Vallet-Regí, J. Gracio, P.A. Marques. *Adv. Health. Mater.*, 2013, **2** 1072–1090.

10. M. Ayán-Varela, J.I. Paredes, L. Guardia, S. Villar-Rodil, J.M. Munuera, M. Díaz-González, C. Fernández-Sánchez, A. Martínez-Alonso, J.M.D. Tascón, *ACS Appl. Mater. Inter.*, 2015, **7**, 10293-10307.

11. S. De, P.J. King, M. Lotya, A. O´Neill, E.M. Doherty, Y. Hernandez, G.S. Duesberg, J.N. Coleman, *Small*, 2010, **6**, 458-464.

12. L. Guardia, M.J. Fernández-Merino, J.I. Paredes, P. Solís-Fernández, S. Villar-Rodil, A. Martínez-Alonso, J.M.D. Tascón, *Carbon*, 2011, **49**, 1653-1662.

13. S. Sampath, A.N. Basuray, K.J. Hartlieb, T. Aytun, S.I. Stupp, J.F. Stoddart. *Adv. Mater.*, 2013, **25**, 2740-2745.

14. V. Chabot, B. Kim, B. Sloper, C. Tzoganakis, A. Yu, *Sci. Reports*, 2013, **3**, 1378.

15. M. Orecchioni, C. Ménard-Moyon, L.G. Delogu, A. Bianco, *Adv. Drug Deliv. Rev.*, 2016, **105**, 163-175.

16. M. Nakayama, *Front. Immunol.*, 2018, **9**, 103.

17. D.M. Mosser, J.P. Edwards, *Nat. Rev. Immunol.*, 2008, **8**, 958–969.

18. D. Reichel, M. Tripathi, J.M. Perez, *Nanotheranostics*, 2019, **3**, 66–88.

19. N.C. Williams, L.A.J. O'Neill, *Front. Immunol.*, 2018, **9**, 141.

20. Y. Nonnenmacher, K. Hiller. *Cell. Mol. Life Sci.*, 2018, **75**, 2093–2109.

21. J. Feng, J. Zhao, F. Hao, Ch. Chen, B. Kishore, H. Tang, *J. Nanopart. Res.*, 2011, **13**, 2049-2062.

22. R. Saborano, T. Wongpinyochit, J. D. Totten, B.F. Johnston, F. P. Seib, I.F. Duarte. *Adv. Health. Mater.*, 2017, **6**, 1601240.

23. J.D. Totten, T. Wongpinyochit, J. Carrola, I.F. Duarte, F.P. Seib, *ACS Appl. Mater. Interfaces*, 2019, **11**, 14515-14525.

24. M. Vila, M.T. Portolés, P.A.A.P. Marques, M.J. Feito, M.C. Matesanz, C. Ramírez-Santillán, G. Gonçalves, S.M.A. Cruz, A. Nieto, M. Vallet-Regí, *Nanotechnology*, 2012, **23**, 465103 (9pp).

25. ISO 10993-5:2009(E). (2009). Biological evaluation of medical devices – Part 5: Tests for in vitro cytotoxicity.

26. H. Suzuki, T. Toyooka, Y. Ibuki, *Environ. Sci. Technol.*, 2007, **41**, 3018-3024.

27. J. Carrola, V. Bastos, J.M. Ferreira de Oliveira, H. Oliveira, C. Santos, A.M. Gil, I.F. Duarte, *Arch. Biochem. Biophys.*, 2016, **589**, 53-61.

28. D.S. Wishart, Y.D. Feunang, A. Marcu, A.C. Guo, K. Liang, R. Vázquez-Fresno, T. Sajed, D. Johnson, C. Li, N. Karu, Z. Sayeeda, E. Lo, N. Assempour, M. Berjanskii, S. Singhal, D. Arndt, Y. Liang, H. Badran, J. Grant, A. Serra-Cayuela, Y. Liu, R. Mandal,

V. Neveu, A. Pon, C. Knox, M. Wilson, C. Manach, A. Scalbert, *Nucleic Acids Res.*, 2018, **46**, 608-617.

29. L. Berben, S.M. Sereika, S. Engberg, *Int. J. Nurs. Stud.*, 2012, **49**, 1039-1047.

30. S.E. Burastero, Z. Magnani, C. Confetti, L. Abbruzzese, S. Oddera, P. Balbo, G.A. Rossi, E. Crimi, *J. Allergy Clin Immunol.*, 1999, **103**, 1136‑1142.

31. T. Rőszer, *Mediators Inflamm.*, 2015, **2015**, 816460.

32. J.I. Paredes, S. Villar-Rodil, *Nanoscale*, 2016, **8**, 15389-15413.

33. D. Li, M.B. Müller, S. Gilje, R.B. Kaner, G.G. Wallace. *Nat. Nanotechnol.*, 2008, **3**, 101–105.

34. C. Backes, K.R. Paton, D. Hanlon, S. Yuan, M.I. Katsnelson, J. Houston, R.J. Smith, D. McCloskey, J.F. Donegan, J.N. Coleman, *Nanoscale*, 2016, **8**, 4311-4323.

35. L.M. Malard, M.A. Pimenta, G. Dresselhaus, M.S. Dresselhaus, *Phys. Rep.*, 2009, **473**, 51-87.

36. A.C. Ferrari, D.M. Basko, *Nat. Nanotechnol.*, 2013, **8**, 235-246.

37. A. Eckmann, A. Felten, A. Mishchenko, L. Britnell, R. Krupke, K.S. Novoselov, C. Casiraghi, *NanoLett.*, 2012, **12**, 3925-3930.

38. K.R. Paton, E. Varrla, C. Backes, R.J. Smith, U. Khan, A. O'Neill, C. Boland, M. Lotya, O.M. Istrate, P. King, T. Higgins, S. Barwich, P. May, P. Puczkarski, I. Ahmed, M. Moebius, H. Pettersson, E. Long, J. Coelho, S.E. O'Brien, E.K. McGuire, B. Mendoza Sanchez, G.S. Duesberg, N. McEvoy, T.J. Pennycook, C. Downing, A. Crossley, V. Nicolosi, J.N. Coleman, *Nat. Mater.*, 2014, **13**, 624–630.

39. M. Lotya, A. Rakovich, J.F. Donegan, J.N. Coleman, *Nanotechnology*, 2013, **24**, 265703.

40. J. Amaro-Gahete, A. Benítez, R. Otero, D. Esquivel, C. Jiménez-Sanchidrián, J. Morales, A. Caballero, F.J. Romero-Salguero, *Nanomaterials – Basel*, 2019, **9**, E152.

41. A.F. Girão, G. Gonçalves, K.S. Bhangra, J.B. Phillips, J. Knowles, G. Otero-Irurueta, M. K. Singh, I. Bdkin, A. Completo, P.A. Marques, *RSC Adv.* 2016, **6**, 49039–49051.

42. H.L. Herd, K.T. Bartlett, J.A. Gustafson, L.D. McGill, H. Ghandehari, *Biomaterials*, 2015, **53**, 574-582.

43. K. Yang, Y. Li, X. Tan, R. Peng, Z. Liu, *Small*, 2013, **9**, 1492–1503.

44. V.C. Sanchez, A. Jachak, R.H. Hurt, A.B. Kane, *Chem. Res. Toxicol.*, 2011, **25**, 15–34.

45. P.C. Rodriguez, A.C. Ochoa, A.A. Al-khami, *Front. Immunol.*, 2017, **8**, 93.

46. D.G. Ryan, L.A.J. O`Neill, *FEBS Lett.*, 2017, **19**, 2992-3006.

47. J. Meiser, L. Krämer, S.C. Sapcariu, N. Battello, J. Ghelfi, A.F. D´Herouel, A. Skupin, K. Hiller, *J. Biol. Chem.*, 2016, **291**, 3932-3946.

48. A.K. Jha, S.C. Huang, A. Sergushichev, V. Lampropoulou, Y. Ivanova, E. Loginicheva, K. Chmielewski, K.M. Stewart, J. Ashall, B. Everts, E.J. Pearce, E.M. Driggers, M.N. Artyomov, *Immunity*, 2015, **42**, 419-430.

49. G.M. Tannahill, A.M. Curtis, J. Adamik, E.M. Palsson-McDermott, A.F. McGettrick, G. Goel, C. Frezza, N.J. Bernard, B. Kelly, N.H. Foley, L. Zheng, A. Gardet, Z. Tong, S.S. Jany, S.C. Corr, M. Haneklaus, B.E. Caffrey, K. Pierce, S. Walmsley, F.C. Beasley, E. Cummins, V. Nizet, M. Whyte, C.T. Taylor, H. Lin, S.L. Masters, E. Gottlieb, V.P. Kelly, C. Clish, P.E. Auron, R.J. Xavier, L.A. O'Neill, *Nature*, 2013, **496**, 238-242.

50. E.L. Mills, D.G. Ryan, H.A. Prag, D. Dikovskaya, D. Menon, Z. Zaslona, M.P. Jedrychowski, A.S.H. Costa, M. Higgins, E. Hams, J. Szpyt, M.C. Runtsch, M.S. King, J.F. McGouran, R. Fischer, B.M. Kessler, A.F. McGettrick, M.M. Hughes, R.G. Carroll, L.M. Booty, E.V. Knatko, P.J. Meakin, M.L.J. Ashford, L.K. Modis, G. Brunori, D.C. Sévin, P.G. Fallon, S.T. Caldwell, E.R.S. Kunji, E.T. Chouchani, C. Frezza C, A.T. Dinkova-Kostova, R.C. Hartley, M.P. Murphy, L.A. O'Neill, *Nature*, 2018, **556**, 113-117.

51. G. Lalwani, M. D´Agati, A.M. Khan, B. Sitharaman, *Adv. Drug Del. Rev.*, 2016, **105**, 109-144.

52. K.M. Rattigan, A.W. Pountain, C. Regnault, F. Achcar, I.M. Vincent, C.S. Goodyear, M.P. Barrett, *PLoS ONE*, 2018, **13**, e0194126.

53. U. Schlattner, M. Tokarska-Schlattner, T. Wallimann, Biochim. *Biophys. Acta (BBA) - Mol. Basis Disease*, 2006, **1762**, 164-180.

54. J.D. Loike, V.F. Kozler, S.C. Silverstein, *J. Biol. Chem.*, 1979, **254**, 9558-9564.

55. S.D. Lamour, B.S. Choi, H.C. Keun, I. Müller, J. Saric, *J. Proteome Res.*, 2012, **11,** 4211-4222.

56. M.M.S. Paula, C.S. Costa, M.C. Baldin, G. Scaini, G.T. Rezin, K. Segala, V. M. Andrade, C.V. Francoc, E.L. Streck, 2009, J. Braz. Chem. Soc., **20**, 1556-1560.

57. S.X. Adamson, R. Wang, W. Wu, B. Cooper, J. Shannahan, *PLoS ONE*, 2018, **13**, e0207042.

58. M.J. Feito, R. Diez-Orejas, M. Cicuéndez, L. Casarrubios, J.M. Rojo, M.T. Portolés, *Colloids Surf. B: Biointerfaces*, 2019, **176**, 96-105.

Figure Captions

Figure 1. Microscopic and spectroscopic characterization of graphene flakes from aqueous FMN-stabilized graphene colloidal dispersions. Red and green traces correspond to PG-FMN (L) and PG-FMN (S), respectively, while black traces correspond to the starting graphite powder. **(A)** UV-vis extinction spectra of FMN-stabilized aqueous graphene colloidal dispersions; **(B)** Representative STEM images of PG-FMN (L) and **(C)** PG-FMN (S) flakes; **(D)** Histograms of lateral size of PG-FMN (L) and **(E)** PG-FMN (S) flakes measured on ~100 objects from the STEM images; **(F)** Raman spectra of graphene films obtained from FMN-stabilized graphene dispersions; **(G)** Normalized, background-subtracted, high resolution core level C 1s spectra of graphene films obtained from FMN-stabilized graphene dispersions.

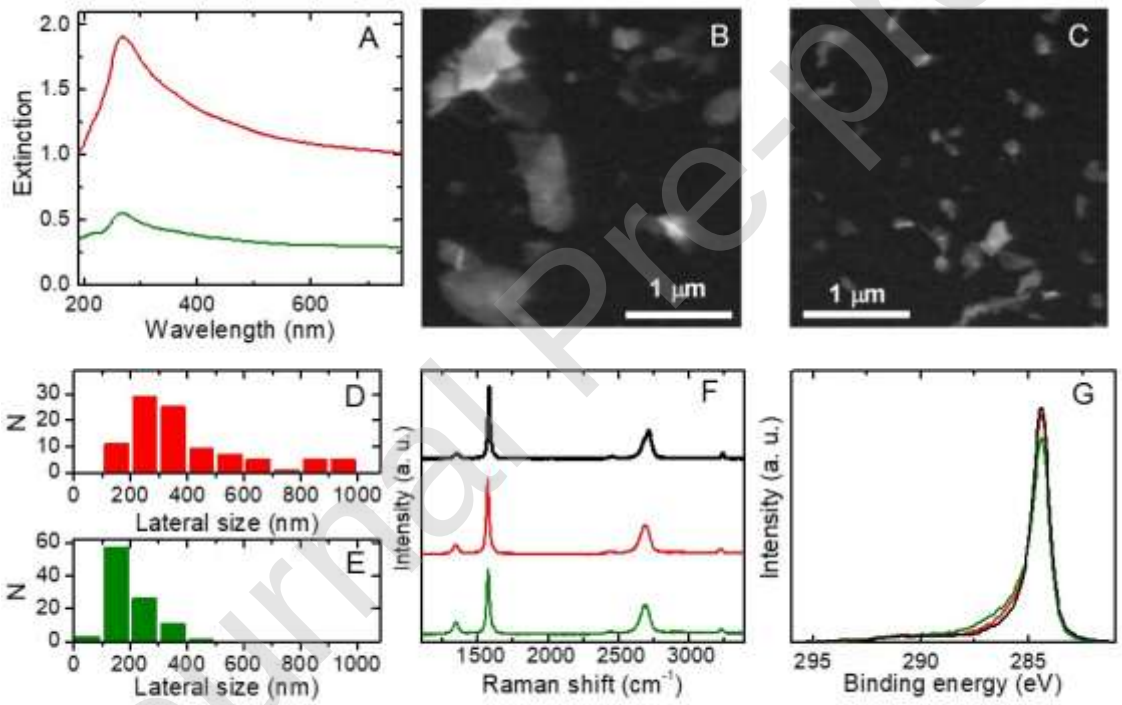

Figure 2. Characterization of GO-PEG. **(A)** AFM representative topographic image of dispersed GO. The graph represents the thickness profile obtained from the white line of the AFM image; **(B)** Particle size distribution of GO obtained by DLS; **(C)** C1s and **(D)** N1s XPS spectra obtained from GO.

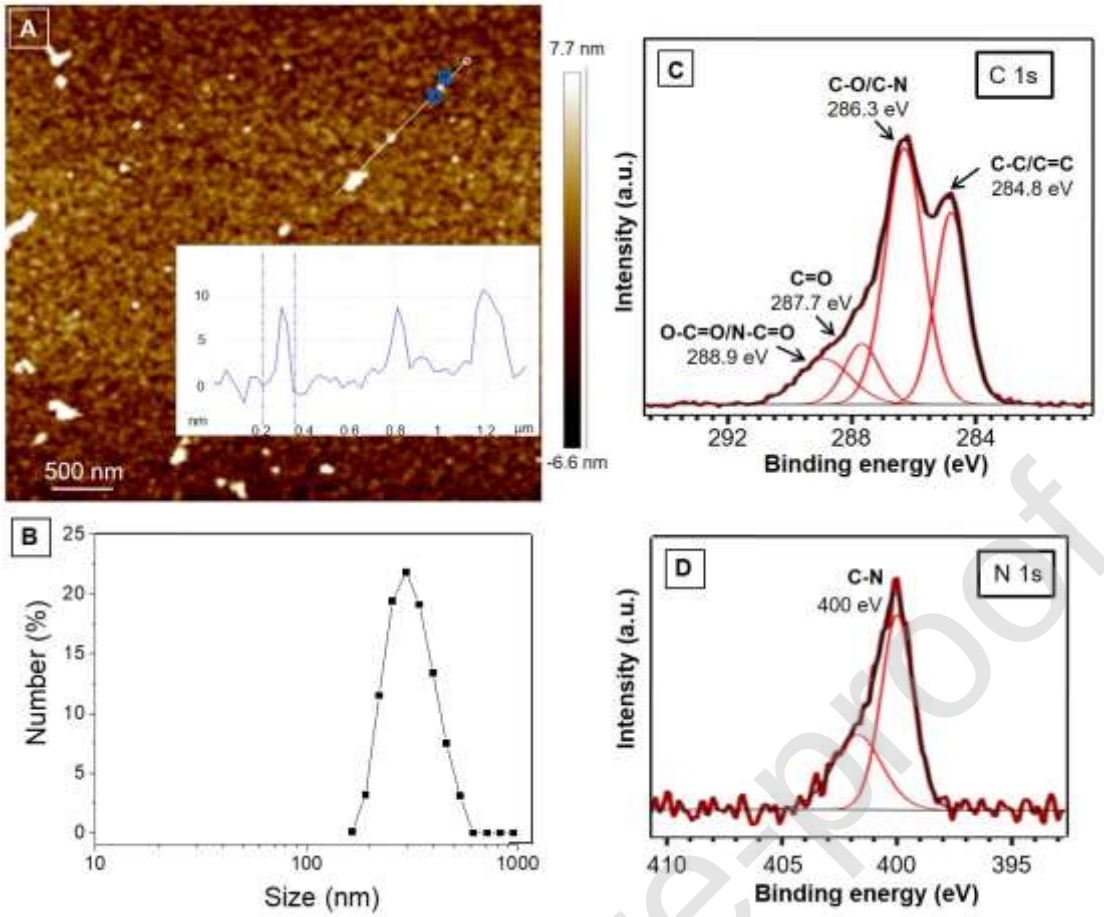

Figure 3. Cell uptake of GBNs by RAW-264.7 macrophages. **(A)** Side angle scatter (SSC-A, internal complexity) *vs.* number of macrophages after 24 h of culture in the absence of nanomaterial (blue profile) and cultured with PG-FMN (L) and PG-FMN (S) nanomaterials (orange and green profiles, respectively). The bar graph (inset) represents the geometric mean of SSC data as mean ± SD, for the culture conditions tested; **(B)** Fluorescence profiles of macrophages cultured for 24 h with GO-PEG-FITC compared to control cells in the absence of nanomaterial (Ctrl). The bar graph (inset) represents the geometric mean of the FITC fluorescence intensity as mean ± SD, for the culture conditions tested. Representative images of cultured RAW-264.7 macrophages after ingestion of GBNs obtained by optical microscopy are also displayed. Statistical significance: *p<0.05, **p<0.01, ***p<0.005.

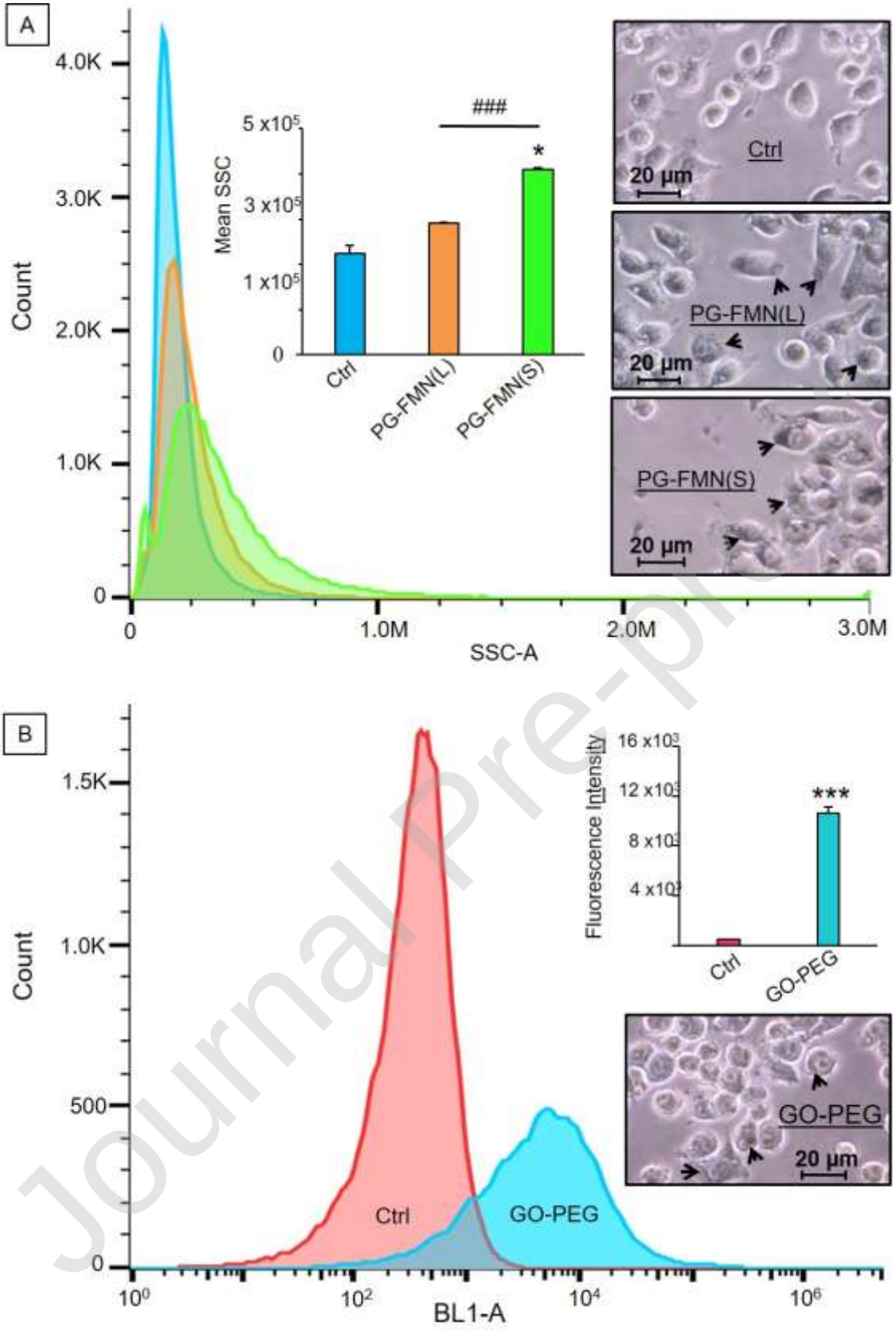

Figure 4. Percentage of variation in nitric oxide production by macrophages incubated with LPS, GO-PEG, PG-FMN (S) and PG-FMN (L) compared to untreated control cells, as assessed by the Griess assay (**p<0.01, ***p<0.005).

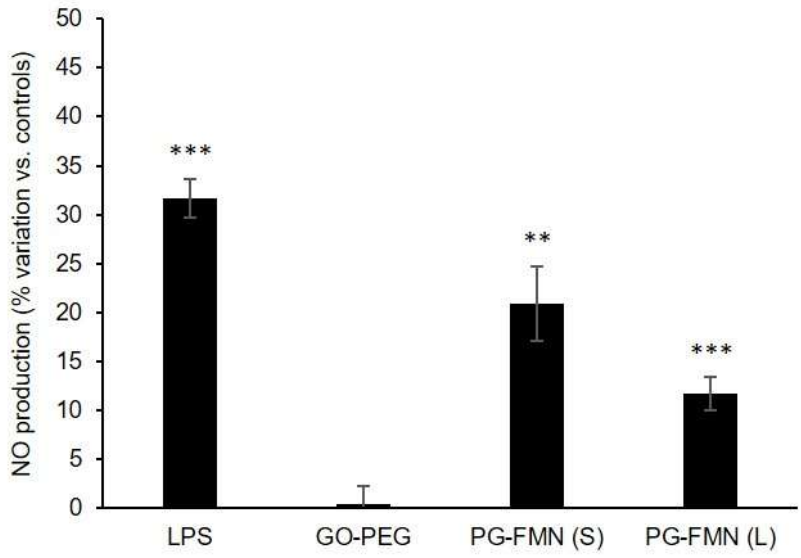

Figure 5. (A) 500 MHz ^{1}H NMR spectrum of a polar extracts from control RAW-264.7 macrophages, with some assigned metabolites indicated, namely: adenosine di/triphosphate (ADP/ATP), alanine (Ala), aspartate (Asp), creatine (Cr), glutamine (Gln), glutamate (Glu), glycine (Gly), glycerophosphocholine (GPC), glutathione (GSH), isoleucine (Ile), leucine (Leu), nicotinamide adenine dinucleotide (NAD^{+}), phosphocholine (PC), phosphocreatine (PCr), taurine (Tau), uridine di/triphosphate (UDP/UTP), valine (Val); **(B)** Heatmap of the main intracellular metabolic variations of RAW-264.7 macrophages exposed to LPS, GO-PEG, PG-FMN (S) and PG-FMN (L), relative to untreated control cells (*p<0.05).

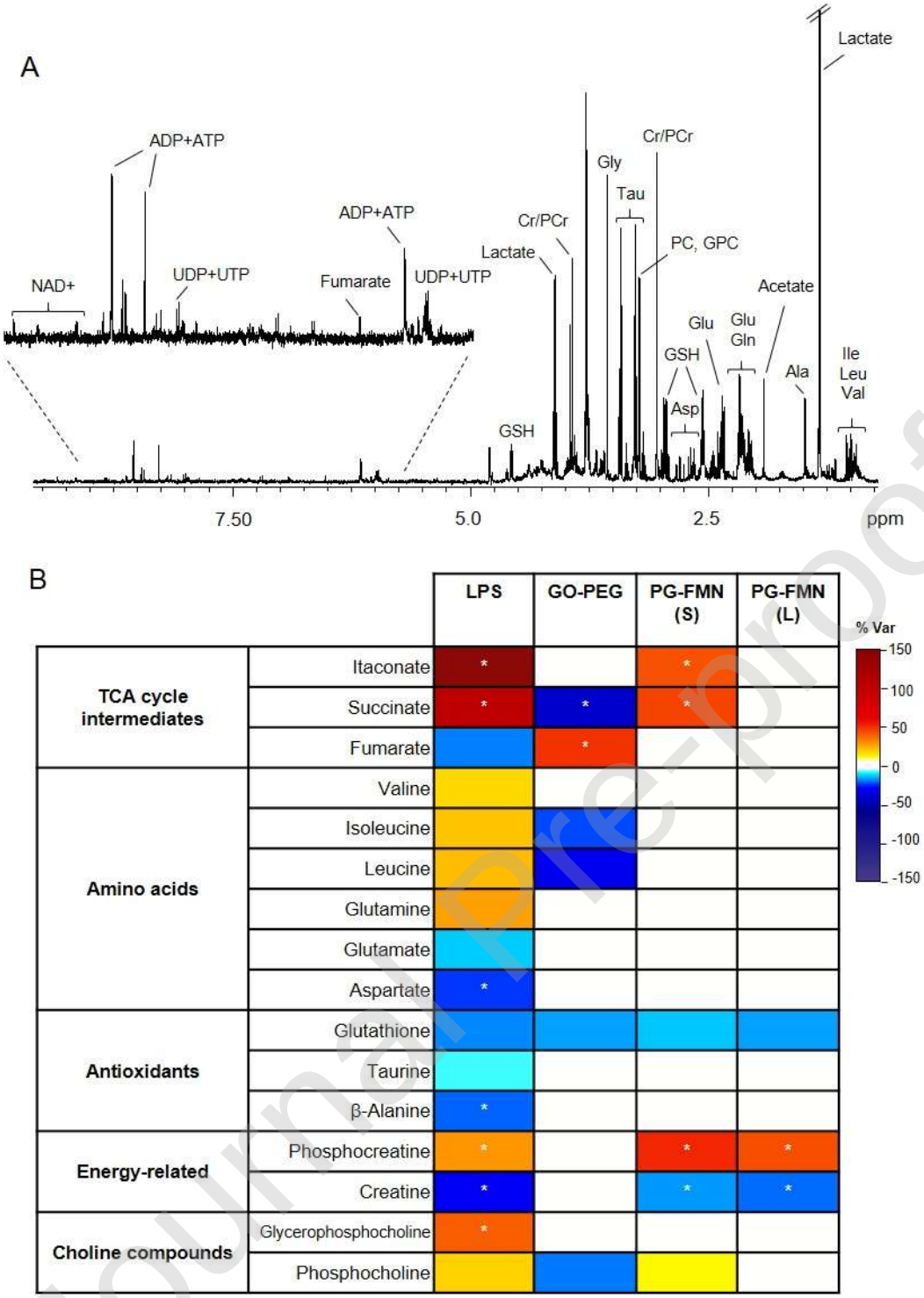

Figure 6. (A) Levels of the pro-inflammatory cytokine TNF-α released by RAW-264.7 macrophages after 24 (***p<0.005) and 48 h ($^{###}p$<0.005) of incubation with GO-PEG; **(B)** Percentage of macrophage populations $CD80^+$ after 24 and 48 h of incubation with GO-PEG-FITC; **p<0.01, control macrophages 48 h *vs* 24 h; $^{##}p$<0.01, macrophages incubated with GO-PEG during 48 h *vs* 24 h, and $^{§}p$<0.05 macrophage populations $CD80^+/GO^+$ 48 h *vs* 24 h. **(C)** Percentage of macrophage populations $CD206^+$ after 24 ($^{&}p$<0.05) and 48 h of incubation with GO-PEG-FITC; *p<0.05, control macrophages 48

h *vs* 24 h; [#] $p<0.05$, macrophages incubated with GO-PEG during 48 h *vs* 24 h and [§] $p<0.05$ macrophage populations $CD206^+/GO^+$ 48 h *vs* 24 h.